DESIGN OF AN AERODYNAMIC BALANCE

Marcos Felipe B.P. de Araujo, mfbpa@ipt.br
Cainã R. Faria, cainarf@ipt.br
Renan V. Arruda, rarruda@ipt.br
Carlos D. Padovezi, padnaval@ipt.br
Institute for Technological Research (IPT), Naval and Ocean Engineering Department, São Paulo, SP, Brazil

Antonio L.C. Mariani, antonio.mariani@poli.usp.br
Escola Politécnica - University of São Paulo, Department of Mechanical Engineering, São Paulo, SP, Brazil

Abstract. *Wind tunnel tests are the basis for the development of aviation industry. More than 70% of tests carried out in wind tunnel require some sort of force measuring device. Once, these instruments were purely mechanical and resembled conventional balances, thus, the name widely used in wind tunnels: Aerodynamic Balance used to measure forces and moments on bodies subjected to a flow. This paper presents the design and calibration method of an Aerodynamic Balance capable of measuring six degrees of freedom (6DOF) related to the aerodynamic forces acting on a scale model to be tested in the wind tunnel of the Institute for Technological Research (IPT). It will be presented the criteria for the choice of material and geometry design of the balance, stress and natural frequency analysis through Finite Elements Method (FEM) in addition to the methodology adopted for calibration. The principle of Aerodynamic Balance presented in this study was based on the Cantilever beam where one end is fixed and the other free. The body to be analyzed is clamped at the free end. The displacement at the free extremity is associated with the forces of drag and lift arising from the fluid flow around the body. The forces are measured by strain levels at specific points in the balance through resistive elements also known as Strain Gauges. These devices exhibit a linear relationship between resistance variation and strain levels. Data of variation of resistance is performed by the Wheatstone bridge, that consist of Strain Gauges and internal resistance of the acquisition data system, providing a variable current that is measured by the galvanometer when deformation occurs in the balance, however, it is noteworthy that this variation is very small. In order to amplify the variable current, four gauges were adopted with full bridges instead of the simple bridge in Wheatstone bridge, quadrupling the current variation.*

Keywords*: Aerodynamic Balance, Strain Gauge, Calibration, Degrees of freedom, Wind Tunnel*

1. INTRODUCTION

One of the most important functions of wind tunnels is to provide estimates of the aerodynamic loads acting on bodies moving through air. These estimates must be measured somehow. The first measurements were obtained using actual balances. Since then, aerodynamic load measurement devices are called aerodynamic balances. Balance types are distinguished by the number of force/moment components which are measured simultaneously– one to six are possible – and the location at which they are placed. Basically, there are two types of wind tunnel balances:

- Internal balance: it is used internally to the model and thus the available space is the primary concern in the project, which is restricted to the diameter of the fuselage of the model. They usually come in the form of stingers and must be attached near the model's center of gravity.
- External balance: available space is not a limiting factor which allows a wide variety of configurations and assemblies of the balance, although there is a concern about the influence on the system's aerodynamics caused by the balance.

Thus, considering the ease of assembly and manufacture of the balance, the choice was the external type. Figure 1 shows an example of an external balance.

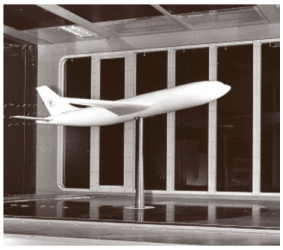

Figure 1 - Example of external balance [Tropea C. *et.al* (2007)]

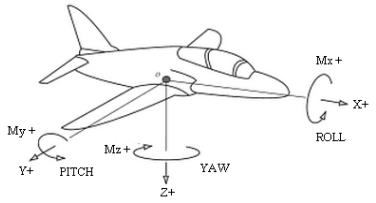

Figure 2 – Coordinate system adopted

This paper presents the design and calibration method of an Aerodynamic Balance capable of measuring six degrees of freedom related to the aerodynamic forces acting on a scale model to be tested in the wind tunnel of the Institute for Technological Research (IPT).

2. DESIGN OF THE AERODYNAMIC BALANCE

Before a balance can be designed, the specifications of the load ranges for the balance are required. The maximum combined loads specify the load ranges for the balance design. The maximum design loads of a balance are defined in various manners. For example, if several loads act simultaneously, then the load range must be specified as the maximum combined load. If the maximum load acts alone, the load range is defined then as the maximum single load.

Usually such single loads do not exist in wind tunnel tests and combined loads must be expected. Such combined loads stress the balance in a much more complicated manner and therefore deserve very careful attention. The stress analysis of the balance has to take into account this situation. Furthermore, the combination of two loads usually requires that the balance carries higher loads.

Initially, estimates were made of the expected maximum forces and moments on a model to be tested in the wind tunnel of the IPT. The composition of forces and moments to define the maximum load acting on the balance was achieved through numerical simulation, which implemented all peak loads encountered at the same time, being able to verify the regions of greatest stress.

2.1. Definition of coordinate systems

The coordinate system adopted, Fig. 2, is fixed to the wind tunnel – the wind axis system – and is aligned to the main flow direction. The lift force is defined as the force on the model acting vertically to the velocity of main flow direction whereas the drag is defined as the force acting parallel to the velocity of the undisturbed stream flow far away from the body. This definition is common all over the world, however, the definition of the positive direction of the forces is not universal. Table 1 presents the definition of positive axis direction.

Table 1 - Definition of positive axis direction

Balance Axis System	Name of Component	Positive Direction
X	Normal force (drag)	In wind
Y	Side force	To starboard
Z	Axial force (lift)	Up
M_X	Rolling moment	Roll to starboard
M_Y	Pitching moment	Turn up
M_Z	Yawing moment	Turn to starboard

An advantage of the coordinate system shown in Fig. 2 is that in the present case the balance stays in the wind axis system and therefore the balance always measures the wind loads. Moreover, for any angle of attack of the aircraft it is possible read the acting forces directly by the balance. If the balance is internal type like, forces should be broken down after the sign reading, since it would follow the angle of the plane.

2.2. Specification of balance load ranges

It was considered an aircraft with maximum wingspan and chord, presence of flaps deflected and maximum angle of attack (before stall). The wingspan of the aircraft is the main dimension that is restricted to the width of the wind tunnel. Given the IPT's wind tunnel section (2 m x 3 m), the maximum acceptable wingspan, according to models previously tested in the wind tunnel, is 1.5 m. The effect of blocking is not discarded and can be corrected by the methodology proposed by Kraft (1983) or Lombardi *et.al* (2001). Considering an aspect ratio (AR) of at least 4, the chord of the wing would be approximately 0.4 m. Thus, the largest wing area that could be tested in the tunnel, focusing on minimizing the effect of the wall, is about 0.6 m². Assuming that the wing is with flaps deflected, the lift coefficient (C_L) can vary from 3.0 to 3.5, depending on Reynolds number. A C_L of this order would produce a drag coefficient (C_D) of 0.4, because a wing with AR=4 has a high induced drag. The moment coefficients of roll, pitch and yaw were assumed, respectively, as C_{Mx}=0.1, C_{My}=0.5 e C_{Mz}=0.05.

The IPT's wind tunnel reaches a maximum flow speed of 18 m/s. For the altitude of São Paulo the average temperature is about 20°C with approximate density (ρ) of 1.02 kg/m³ which results in a dynamic pressure:

$$q = 0.5\rho V^2 \tag{1}$$

Equal to 165 Pa. Thus, the forces and moments that could be expected in a tunnel as the one located at IPT are presented in Tab. 2.

Table 2 – Estimate of forces

M_X [N.m]	M_Y [N.m]	M_Z [N.m]	D [N]	L [N]	F_Y [N]
14,9	19,8	7,4	39,6	297,0	17,0

Where *D* and *L* are the drag and lift forces acting in the model, F_Y is the lateral force estimated by Mutschler (2005), *S* is the plan form area and *c* is the length of the chord of the wing:

$$M_X = C_{M_X} qSc \tag{2}$$

$$M_Y = C_{M_Y} qSc \tag{3}$$

$$M_Z = C_{M_Z} qSc \tag{4}$$

$$L = C_L qS \tag{5}$$

$$D = C_D qS \tag{6}$$

It is observed from Tab. 2 that the active forces have different orders of magnitude, which results in different orders of magnitude for the bending moments. Thus, it is interesting that each section of the balance, where the strain measurement devices (Strain Gauges) will be installed, has different moment of inertia for each situation. For ease in manufacturing stage and better position of the Strain Gauges to the direction of deformation derived from forces acting on the balance, rectangular sections were adopted. The Gauges used were of 120 Ω with axial grid configuration for forces and moments, while the torsion was measured by a Gauge Rosette type. The Gauges are read by an acquisition data system and within this system there is the formation of a Wheatstone bridge. In order to amplify the variable current, four Gauge full bridges were adopted instead of the simple bridge in Wheatstone bridge, quadrupling the current variation.

At this stage of the project the maximum loads are already defined, enabling calculation of the dimensions of the balance.

2.3. Definition of the geometry of the balance

In general, the structures of the aerodynamic balances are metal alloys whose definition of material depends on the level of stress that will be achieved during the tests. In the present work the stresses arising from aerodynamic forces and moments are: lift, drag and lateral force and moment of pitch, roll and yaw.

2.3.1. Choice of material

According to Tropea *et.al* (2007) the balance must have the highest natural frequency of structural vibration as possible, which improves their sensitivity. The material that makes it up should be light and stiff and should present low hysteresis. Tropea *et.al* (2007) says it is advisable that the active stress concerning the aerodynamic forces to be 3 to 5 times smaller than the yield stress of material. Moreover, for conditions of high stress level metals with higher Young's modulus (*E*) such as Titanium and Copper-Beryllium are used, while for a low stress level, which is the case for models tested in IPT's wind tunnel, aluminum is a good choice.

So, the material chosen was the aeronautical aluminum (Al7075-T651), because as mentioned earlier there is no need to use a robust material and, furthermore, it presents the lowest feasible cost of manufacturing.

Aluminum alloys of aviation series (alloys of the 2XXX and 7XXX series) have as main characteristics the high levels of mechanical resistance that, combined with low density and ease of metal forming and machining, transform the aluminum into one of the best options for manufacture of aircraft structures and devices.

The data regarding the chosen material, Schmolz (2010), are shown in Tab. 3.

Table 3 – Properties of aluminum Al7075-T651

Yield strength [MPa]	Young's modulus [MPa]	Hardness Brinell [HB]	Machinability
260-470	72000	104-161	Good

With possession of the elastic modulus and the maximum forces, acting as shown previously, it was possible to define the structure of the section where the Gauges were positioned.

2.3.2. Definition of the main body section

The balance in project consists of two parts: the main body, which measures the moments and torsion, and load cell, which measures the tension and compression of the balance. Typically, the best balance structure is obtained by manufacturing a balance from a single piece of material. This prevents the appearance of non-linear characteristics as well as hysteresis which could arise at joints or welds. However, the need to manufacture from a single piece of material limits the design significantly. Still, the main body was manufactured from a single piece of metal.

Based on previously IPT's balance projects, it was defined the length of the main body as 200 mm. However, by restrictions imposed by the acquisition of material the length of the balance is 195 mm. Figure 3 shows a CAD drawing and a photo of the main body.

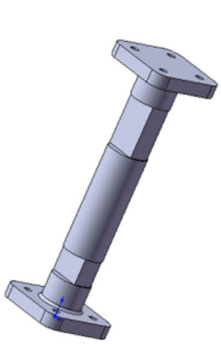

(a) CAD drawing

(b) Main body instrumented

Figure 3 – Main body of the balance

It is observed in Fig. 3 that the main body has two bases joined by a cylindrical rod with notches at certain points which will allocate the Strain Gauges. The foundations have the scale thickness of 10 mm (this measure is based on the balances found in the IPT) whose geometries are square, facilitating the alignment of the reference strain with the acting force. There is a question about the aerodynamics of the bases, because the square section could lead to disruptions in the flow that could be reduced if circular section were used. However, the balance will influence the flow regardless of the section adopted for the foundations and in this case a fairing system could be coupled to the balance. Still, care was taken to round the corners of the bases.

As mentioned earlier it is advisable that the yield stress of the material should be 3 to 5 times the active stress, i.e. stress must remain in the elastic region where is valid the Hooke's law, where σ is the stress and ε is the deformation:

$$\sigma = E\varepsilon \tag{7}$$

The yield stress of Al7075 is assumed as the average limit presented in Tab. 3, i.e. 365 MPa and also the safety factor is 4.Thus, the stresses acting should be a maximum of 91.25 MPa.

$$\sigma = \frac{My_{ln}}{I} \tag{8}$$

Using Eq. (8), where M is the acting moment, together with the estimate of the forces acting on the model, Tab. 2, it is possible to determine the inertia and dimensions of the rectangular section corresponding to the positions of the Gauges. With the simple application of Eq. (8) it is possible to find the relationship between the height of the neutral axis and the inertia of the section for each condition of maximum bending moment, being the same for both sections:

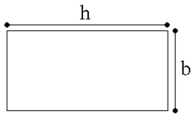

Figure 4 – Rectangular section in the position of Gauges

Where *b* and *h* must be greater than the width of the pair of Strain Gauges used, equivalent to 12 mm.

The inertia of the section and height of the neutral axis to measure the lateral force are given respectively by:

$$I = \frac{hb^3}{12} \tag{9}$$

$$y_{ln} = \frac{b}{2} \tag{10}$$

Similarly, one can use Eq. (9) and Eq. (10) for the case of drag force, but with the inversions of *h* by *b*. Thus the values of *h* and *b* found are respectively equal to 25 mm and 6 mm. However, as a matter of using full bridge, it was necessary that the value of *b* was greater. So was chosen that value of *b* = 15 mm because of the width of Gauges adopted (one beside the other).

It was considered that the centers of the Gauges were at a minimum distance of 40 mm from the ends (bases) of the balance to facilitate the attachment of wires and connections of the Gauges, maximizing the distance between them. The greater the distance between the Gauges, the smaller is the sensitivity to changes and consequently to errors.

It is observed that the sections where the Gauges will be applied have different lengths because in the top recess of Fig. 3, in addition to the Gauges, Rosettes also will be applied. The length of upper and lower recesses are respectively 40 mm and 20 mm, considering the length of the Gauges and diameter of the Rosettes up to 15 mm. Figure 5 shows the Gauges and Rosettes positioning in balance body.

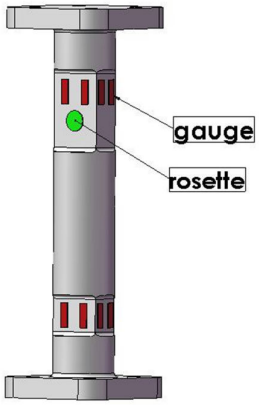

Figure 5 - Balance body with gauges

During the design of the balance in CAD, it was found that due to restrictions of the values of *b* and the diameter of the balance, for which was adopted as 30 mm, the value of *h* showed greater dimension than the pre-established (26 mm), but it does not affect the results. The holes for the fixing of the balance are 6 mm and their centers occupy the vertices of a square of side 40 mm.

2.3.3. Definition of the load cell

The load cell consists of a standard cubic load cell, denominated here as block cell or block, used in the laboratory of marine engineering (IPT) and two angles that united to the block cell form an "s" load cell. The block cell has been designed so that isolated moments act on it. The block is composed by ASTM A1020 while the angles are composed of Al7075. It was observed, in a brief analysis, that even with the mounting of the load cell the reading of moment was negligible. Figure 6 presents a sequence of the load cell assembly. The Strain Gauges are positioned in the region highlighted at the block (a).

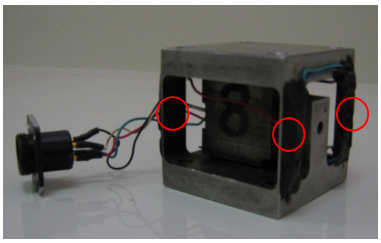

(a) Block cell

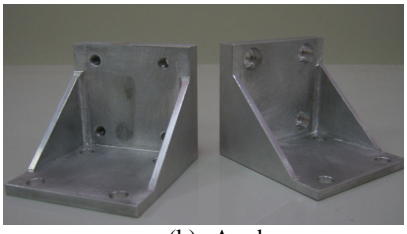

(b) Angles

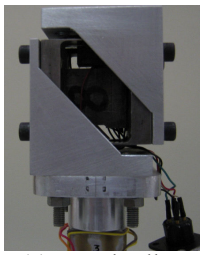

(c) Load cell

Figure 6 – Load cell assembly

2.4. Analysis of bending and torsion of the main body

Prior bend and torsion analysis were performed to check the behavior of the balance in operation. Furthermore, a finite elements analysis was performed in order to verify the maximum stresses and natural vibration models that the balance would be subject to.

2.4.1. Analytical approach of bend and torsion

For the analytical approach, the balance was considered a single beam without the block, but with 0.23 m length. Figure 7 shows the adopted geometry.

A clamped beam mode was used, like illustrated in Fig. 8. The loads responsible for bending in X are drag and pitch moment, and in Y are side force and roll moment, Fig. 2. Undervaluing the normal and shear forces contribution in the strain energy, for a uniform section beam:

$$\delta_B = \frac{\partial U}{\partial F} = \frac{1}{EI}\left(\frac{ML^2}{2} + \frac{FL^3}{3}\right) \tag{11}$$

$$\theta_B = \frac{\partial U}{\partial M} = \frac{1}{EI}\left(ML + \frac{FL^2}{2}\right) \tag{12}$$

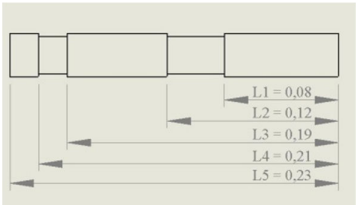

Figure 7 – Geometry adopted for the analysis

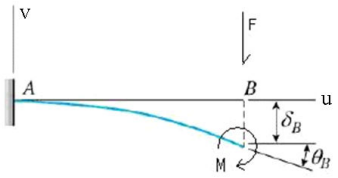

Figure 8 – Clamped beam model

Where δ_B is the deflection of the beam, θ_B is the bending angle and U is the total strain energy.

However, as the balance has a variable transverse section, Fig. 7, the right formulation is given by:

$$\delta_B = \frac{\partial U}{\partial F} = \frac{1}{EI_C}\left(\frac{M({L_1}^2 + {L_3}^2 + {L_5}^2 - {L_2}^2 - {L_4}^2)}{2} + \frac{F({L_1}^3 + {L_3}^3 + {L_5}^3 - {L_2}^3 - {L_4}^3)}{3}\right) + \frac{1}{EI_R}\left(\frac{M({L_2}^2 + {L_4}^2 - {L_1}^2 - {L_3}^2)}{2} + \frac{F({L_2}^3 + {L_4}^3 - {L_1}^3 - {L_3}^3)}{3}\right) \tag{13}$$

$$\theta_B = \frac{\partial U}{\partial M} = \frac{1}{EI_C}\left(M(L_1 + L_3 + L_5 - L_2 - L_4) + \frac{F({L_1}^2 + {L_3}^2 + {L_5}^2 - {L_2}^2 - {L_4}^2)}{2}\right) + \frac{1}{EI_R}\left(M(L_2 + L_4 - L_1 - L_3) + \frac{F({L_2}^2 + {L_4}^2 - {L_1}^2 - {L_3}^2)}{2}\right) \tag{14}$$

Where I_C corresponds to the circular section's transverse inertia moment and I_R to the rectangular section. Replacing the loads values prior estimated and the balance material properties, we have that δ_X = 0.30 mm, θ_X = 0.0024 rad = 0.14°, δ_Y = 0.38 mm and θ_Y = 0.0029 rad = 0.17°.

For the torsion analysis, a free warping beam model was used. According to Timoshenko (1933), for this case the beam torsion angle is given by:

$$\emptyset = \frac{TL}{GI_T} \tag{15}$$

Where I_T corresponds to the section's torsion moment:

$$I_T = \frac{\pi d^4}{32} \tag{16}$$

But for the rectangular section:

$$I_T = 16a^3c\left(\frac{1}{3} - \frac{64a}{\pi^5 c}\sum_{m=0}^{\infty}\frac{\tanh(\lambda_m c)}{(2m+1)^5}\right) \tag{17}$$

Where: $\lambda_m = \frac{\pi}{2a}(2m+1)$, $a = \frac{h}{2} = 12.99\ mm$ and $c = \frac{b}{2} = 7.5\ mm$.
So, the beam total torsion angle can be evaluated like the sum of torsion angles by each stretches:

$$\phi = \frac{T}{G}\left(\frac{L_5 - L_4}{I_{T-circ}} + \frac{L_4 - L_3}{I_{T-ret}} + \frac{L_3 - L_2}{I_{T-circ}} + \frac{L_2 - L_1}{I_{T-ret}} + \frac{L_1}{I_{T-circ}}\right) = 0.0033\ rad = 0.19°$$

3. ANALYSIS OF BALANCE LOAD RANGES BY FINITE ELEMENT METHOD

3.1. Structural analysis

In finite element analysis was created a condition in which the balance supports the maximum efforts of three moments and three forces in *X*, *Y* and *Z* axes, Tab. 2. The basis of the balance was considered clamped and all forces and moments were applied on the upper surface where the model is fixed. Figure 9 presents the numerical results for the static structural analysis of the balance. It is worth mentioning that the main body mass is 0.458 kg and the load cell is 0.777 kg (mass of the block equal to 0.510 kg), resulting in 1.235 kg.

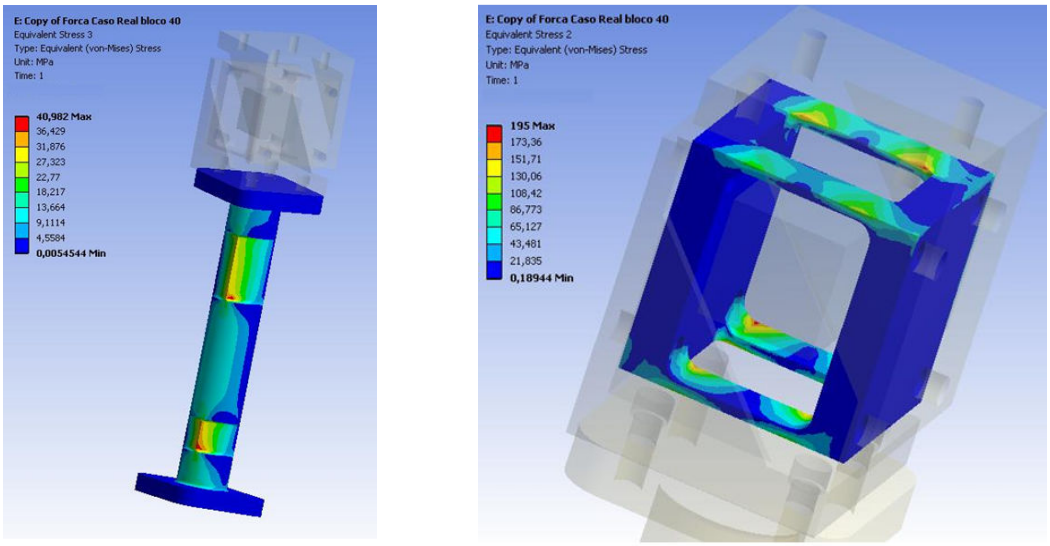

(a) Main body FEM (b) Block cell FEM

Figure 9 – Static structural analysis of the balance

It was found that the block, that compose the load cell, presented stress near the yield stress of the material, 195 MPa, Fig. 9 (b). This is due to the fact that the block cell did not take into account a safety factor as suggested Tropea et.al (2007). Thus, some dimensions of the block could be modified so as not to produce more acting stresses near the yield stress, completing the structural analysis of the balance.

3.2. Modal analysis

The mesh used in modal analysis, as well as structural analysis, consisted of 93.266 tetrahedral solid elements totaling 147.372 nodes. Figure 10 presents the numerical results for the modal analysis of the balance.

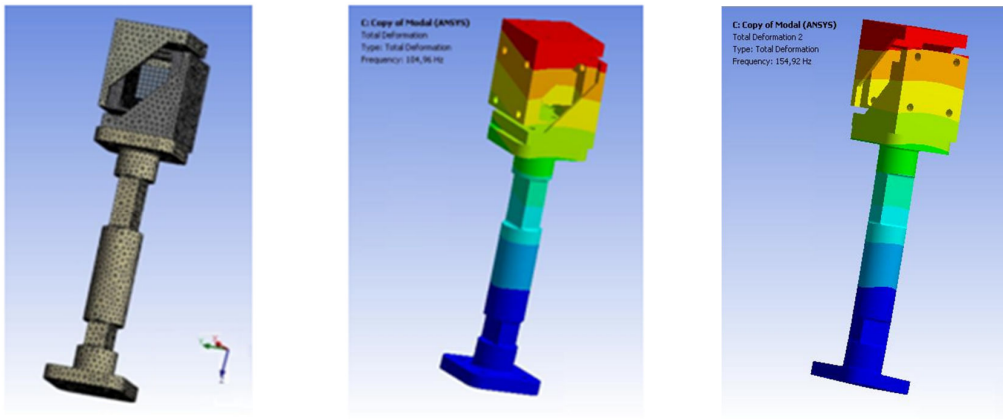

(a) Mesh used (b) Vibration mode 1 (c) Vibration mode 2

Figure 10 – Modal analysis of the balance

The modal analysis showed the natural frequency of 105 Hz for the vibration mode 1 and 155 Hz for the vibration mode 2. It is believed that both frequencies are appropriate for the type of test to be conducted in the wind tunnel.

4. CALIBRATION

In an ideal case the strains presented by the balance and identified by the Strain Gauges are proportional to the applied loads. However, due to the imperfection of balance design and manufacturing, and the combined loading condition during tests, there is a degree of dependence between the component forces of the measure device.

Figure 11 shows how the strains occasioned by a load can interfere in a second component reading.

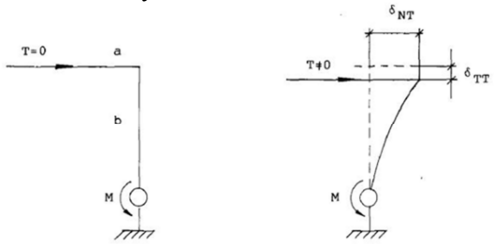

Figure 11 – Strains that interfere in a second component reading [Fristedt (1993)]

In this example, when T is different from zero, the moment recorded by the Strain Gauge has a contribution given by the axial strain caused by this moment. So:

$$M = T(b - \delta_{TT}) \tag{18}$$

For the device correct functioning, it is necessary a formulation that takes into account the interactions between the loads to generate a calibration matrix.

According to Fristedt (1993) a second order analysis is enough to obtain good accuracy. Moreover, an approach that takes in account cross-terms with the signal modules was adopted, because according to the table presented in Fig. 12, it has an advantage over the method that interprets the cross-terms just with the relative values.

	Standard Error [%]						
	HX	HY	HZ	Hl	Hm	Hn	Average
6 coeff.	0.43583	0.16990	0.13213	0.60045	0.07482	0.14332	0.25941
27 coeff.	0.05860	0.11663	0.08537	0.21537	0.06149	0.09848	0.10599
33 coeff.	0.05665	0.11216	0.08473	0.21040	0.05645	0.09321	0.10227
84 coeff.	0.05187	0.08055	0.07129	0.14107	0.04508	0.06077	0.07511
96 coeff.	0.05079	0.07794	0.06952	0.13771	0.04389	0.05986	0.07329

Figure 12 – Standard error for the [H]=[C][R] balance calibration model with 1886 points [Leung and Link (1999)]

The formulations using 27 and 84 coefficients are the second order formulations. However, when the cross-terms are evaluated with the modules, it is necessary 84 coefficients. There is a decrease of 0.03% in the standard error average comparing the 84 and the 27 coefficients formulations.

For example, if H_i is some load component:

$$\begin{aligned} H_i = {} & C_{i,1}R_1 + C_{i,2}R_2 + C_{i,3}R_3 + C_{i,4}R_4 + C_{i,5}R_5 + C_{i,6}R_6 + C_{i,|1|}|R_1| + C_{i,|2|}|R_2| + C_{i,|3|}|R_3| + C_{i,|4|}|R_4| \\ & + C_{i,|5|}|R_5| + C_{i,|6|}|R_6| + C_{i,12}R_1R_2 + C_{i,13}R_1R_3 + C_{i,14}R_1R_4 + C_{i,15}R_1R_5 + C_{i,16}R_1R_6 \\ & + C_{i,23}R_2R_3 + C_{i,24}R_2R_4 + C_{i,25}R_2R_5 + C_{i,26}R_2R_6 + C_{i,34}R_3R_4 + C_{i,35}R_3R_5 + C_{i,36}R_3R_6 \\ & + C_{i,45}R_4R_5 + C_{i,46}R_4R_6 + C_{i,56}R_5R_6 + C_{i,|12|}|R_1R_2| + C_{i,|13|}|R_1R_3| + C_{i,|14|}|R_1R_4| \\ & + C_{i,|15|}|R_1R_5| + C_{i,|16|}|R_1R_6| + C_{i,|23|}|R_2R_3| + C_{i,|24|}|R_2R_4| + C_{i,|25|}|R_2R_5| \\ & + C_{i,|26|}|R_2R_6| + C_{i,|34|}|R_3R_4| + C_{i,|35|}|R_3R_5| + C_{i,|36|}|R_3R_6| + C_{i,|45|}|R_4R_5| \\ & + C_{i,|46|}|R_4R_6| + C_{i,|56|}|R_5R_6| + C_{i,|1|2}|R_1|R_2 + C_{i,|1|3}|R_1|R_3 + C_{i,|1|4}|R_1|R_4 \\ & + C_{i,|1|5}|R_1|R_5 + C_{i,|1|6}|R_1|R_6 + C_{i,|2|3}|R_2|R_3 + C_{i,|2|4}|R_2|R_4 + C_{i,|2|5}|R_2|R_5 \\ & + C_{i,|2|6}|R_2|R_6 + C_{i,|3|4}|R_3|R_4 + C_{i,|3|5}|R_3|R_5 + C_{i,|3|6}|R_3|R_6 + C_{i,|4|5}|R_4|R_5 \\ & + C_{i,|4|6}|R_4|R_6 + C_{i,|5|6}|R_5|R_6 + C_{i,1|2|}R_1|R_2| + C_{i,1|3|}R_1|R_3| + C_{i,1|4|}R_1|R_4| \\ & + C_{i,1|5|}R_1|R_5| + C_{i,1|6|}R_1|R_6| + C_{i,2|3|}R_2|R_3| + C_{i,2|4|}R_2|R_4| + C_{i,2|5|}R_2|R_5| \\ & + C_{i,2|6|}R_2|R_6| + C_{i,3|4|}R_3|R_4| + C_{i,3|5|}R_3|R_5| + C_{i,3|6|}R_3|R_6| + C_{i,4|5|}R_4|R_5| \\ & + C_{i,4|6|}R_4|R_6| + C_{i,5|6|}R_5|R_6| + C_{i,11}{R_1}^2 + C_{i,22}{R_2}^2 + C_{i,33}{R_3}^2 + C_{i,44}{R_4}^2 + C_{i,55}{R_5}^2 \\ & + C_{i,66}{R_6}^2 + C_{i,1|1|}R_1|R_1| + C_{i,2|2|}R_2|R_2| + C_{i,3|3|}R_3|R_3| + C_{i,4|4|}R_4|R_4| + C_{i,5|5|}R_5|R_5| \\ & + C_{i,6|6|}R_6|R_6| \end{aligned} \tag{19}$$

In the matrix form:

$$[\mathrm{H}] = [\mathrm{C}][\mathrm{R}] \tag{20}$$

Where $[H]_{6x1}$ is the efforts matrix, $[C]_{6x84}$ is the coefficients matrix and $[R]_{84x1}$ is the Strain Gauges reading matrix. The $|R_i|$ terms correspond to the modulus of the reading signals.

To obtain the 504 coefficients matrix $[C]$, the least squares method will be utilized. According to Leung and Link (1999) results, for a sample with nearly 2000 measures, the standard error is about 0.07%. Therefore, the balance calibration will be scaled respecting this minimum measures number.

So, using the least squares method, if p is the number of measures:

$$[\mathrm{C}]^{\mathrm{t}}=[\mathrm{E}]^{-1}[\mathrm{A}] \tag{21}$$

$$[E] = \begin{bmatrix} \sum R_{1,p}R_{1,p} & \sum R_{1,p}R_{2,p} & \sum R_{1,p}R_{3,p} & \Lambda & \sum R_{1,p}R_{5,p}|R_{5,p}| & \sum R_{1,p}R_{6,p}|R_{6,p}| \\ \sum R_{2,p}R_{1,p} & \sum R_{2,p}R_{2,p} & \sum R_{2,p}R_{3,p} & \Lambda & \sum R_{2,p}R_{5,p}|R_{5,p}| & \sum R_{2,p}R_{6,p}|R_{6,p}| \\ \sum R_{3,p}R_{1,p} & \sum R_{3,p}R_{2,p} & \sum R_{3,p}R_{3,p} & \Lambda & \sum R_{3,p}R_{5,p}|R_{5,p}| & \sum R_{3,p}R_{6,p}|R_{6,p}| \\ \mathrm{M} & \mathrm{M} & \mathrm{M} & & \mathrm{M} & \mathrm{M} \\ \sum R_{5,p}^2R_{1,p} & \sum R_{5,p}^2R_{2,p} & \sum R_{5,p}^2R_{3,p} & \Lambda & \sum R_{5,p}^2R_{5,p}|R_{5,p}| & \sum R_{5,p}^2R_{6,p}|R_{6,p}| \\ \sum R_{6,p}^2R_{1,p} & \sum R_{6,p}^2R_{2,p} & \sum R_{6,p}^2R_{3,p} & \Lambda & \sum R_{6,p}^2R_{5,p}|R_{5,p}| & \sum R_{6,p}^2R_{6,p}|R_{6,p}| \end{bmatrix} \tag{22}$$

$$[A] = \begin{bmatrix} \sum R_{1,p}H_{1,p} & \sum R_{1,p}H_{2,p} & \sum R_{1,p}H_{3,p} & \Lambda & \sum R_{1,p}H_{5,p} & \sum R_{1,p}H_{6,p} \\ \sum R_{2,p}H_{1,p} & \sum R_{2,p}H_{2,p} & \sum R_{2,p}H_{3,p} & \Lambda & \sum R_{2,p}H_{5,p} & \sum R_{2,p}H_{6,p} \\ \sum R_{3,p}H_{1,p} & \sum R_{3,p}H_{2,p} & \sum R_{3,p}H_{3,p} & \Lambda & \sum R_{3,p}H_{5,p} & \sum R_{3,p}H_{6,p} \\ \mathrm{M} & \mathrm{M} & \mathrm{M} & & \mathrm{M} & \mathrm{M} \\ \sum R_{5,p}|R_{5,p}|H_{1,p} & \sum R_{5,p}|R_{5,p}|H_{2,p} & \sum R_{5,p}|R_{5,p}|H_{3,p} & \Lambda & \sum R_{5,p}|R_{5,p}|H_{5,p} & \sum R_{5,p}|R_{5,p}|H_{6,p} \\ \sum R_{6,p}|R_{6,p}|H_{1,p} & \sum R_{6,p}|R_{6,p}|H_{2,p} & \sum R_{6,p}|R_{6,p}|H_{3,p} & \Lambda & \sum R_{6,p}|R_{6,p}|H_{5,p} & \sum R_{6,p}|R_{6,p}|H_{6,p} \end{bmatrix} \tag{23}$$

$$[C]^t = \begin{bmatrix} C_{1,1} & C_{2,1} & C_{3,1} & C_{4,1} & C_{5,1} & C_{6,1} \\ C_{1,2} & C_{2,2} & C_{3,2} & C_{4,2} & C_{5,2} & C_{6,2} \\ \mathrm{M} & \mathrm{M} & \mathrm{M} & \mathrm{M} & \mathrm{M} & \mathrm{M} \\ C_{1,5|5|} & C_{2,5|5|} & C_{3,5|5|} & C_{4,5|5|} & C_{5,5|5|} & C_{6,5|5|} \\ C_{1,6|6|} & C_{2,6|6|} & C_{3,6|6|} & C_{4,6|6|} & C_{5,6|6|} & C_{6,6|6|} \end{bmatrix} \tag{24}$$

Finally to obtain the loads values:

$$\begin{bmatrix} H_1 \\ H_2 \\ H_3 \\ H_4 \\ H_5 \\ H_6 \end{bmatrix} = [C] \begin{bmatrix} R_1 \\ R_2 \\ R_3 \\ M \\ R_5|R_5| \\ R_6|R_6| \end{bmatrix} \tag{25}$$

5. CONCLUSIONS

This work presented the design of an aerodynamic balance of 6 degrees of freedom to monitor forces and moments on models in IPT's wind tunnel. The balance is composed of two parts being the first one, called main body, massive composed of aluminum Al7075 and the second part consists of ASTM A1020 (block) and Al7075 (angle), forming the "s" load cell.

As an estimate of the maximum loads, the maximum dimensions of a model that would be tested in the IPT's wind tunnel was used. The corrections of the wall effect could be realized according to Kraft (1983) or Lombardi *et.al* (2001). It was possible to define the geometry and material of the balance according to the assumption that the yield stress of the material should be 3 to 5 times the tension acting on the balance, Tropea et.al (2007).

A brief analysis of bending and torsion of the balance was performed in which maximum results were obtained: deflection of δ_Y = 0.38 mm, bending angle θ_Y = 0.17° and torsion angle of 0.19°. These values were considered appropriate for the balance. The stress distribution for the combination of loads was investigated numerically as well as the modes of vibration of the balance. It was found that the main body of the balance behaved accordingly to expected, however, the block cell had stresses close to the yield stress of ASTM A1020 (195 MPa). Thus, it is advisable to use a more stiff block. The vibration modes of the balance showed a high frequency, as desired, being 105 Hz at the first mode and 155 Hz at the second vibration mode.

Finally, was presented the calibration methodology adopted in which 84 calibration coefficients were used.

There is still a need to conduct tests with models in wind tunnel in order to ascertain the effectiveness of the balance in measuring efforts. Moreover, different materials could be used to manufacture new balances like Copper-Beryllium and new geometries could be tried like the load cell coupled to the mean body. In future studies it will also be analyzed calibration devices and comparisons will be made between the balance projected and commercial ones.

6. ACKNOWLEDGEMENTS

The authors wish to thank the technical team of the Laboratory of Instrumentation in Fluid Mechanics at Escola Politécnica, of the University of São Paulo (USP) for providing the material and the manufacturing process of the balance.

7. REFERENCES

Fristedt K., 1993, "A calibration model of six component internal wind-tunnel balance of the bending-beam type", Elsevier, Stockholm, Sweden, pp 107-118.

Kraft E.M., 1983, "An overview of approaches and issues for wall interference assessment and correction," *NASA CP-2319*.

Leung *S*.Y.F., Link Y.Y., 1999, "Comparison and Analysis of Strain Gauge Balance - Calibration Matrix Mathematical Models", DSTO Aeronautical and Maritime Research Laboratory, Melbourne, Australia.

Lombardi G., Salvetti M.V., Morelli M., 2001, "Correction of the Wall Interference Effects in Wind Tunnel Experiments", Department of Aerospace Engineering, University of Pisa, Italy.

Mutschler F.A., 2005, "Balança aerodinâmica de seis componentes", Trabalho de formatura, Universidade de São Paulo, São Paulo, Brazil.

Schmolz+Bickenbach do Brasil. "Propriedades do Al7075". 30 April 2010, <www.schmolz- bickenbach.com.br/index.php?id=3578>

Timoshenko S.,1933, "Theory of Elasticity" University of Michigan.

Tropea C., Yarin A.L., Foss J.F., 2007, "Springer Handbook of Experimental Fluid Mechanics", Ed. Springer, Berlim, Germany.

8. RESPONSIBILITY NOTICE

The authors are the only responsible for the printed material included in this paper.